Quantitative polarized light microscopy of human cochlear sections

Jacob CM Low[1], Thomas J Ober[2], Gareth H McKinley[2], Konstantina M Stankovic[3,4]

[1] The University of Manchester, Oxford Road, Manchester, M13 9PL, UK

[2] Massachusetts Institute of Technology, Department of Mechanical Engineering, 77 Massachusetts Avenue, Cambridge, Massachusetts 02139, USA

[3] Massachusetts Eye and Ear, Department of Otolaryngology and Eaton Peabody Laboratories, 243 Charles Street, Boston, Massachusetts 02114, USA

[4]Department of Otology and Laryngology, Harvard Medical School, Boston, Massachusetts, USA

Corresponding author:
Konstantina Stankovic
Massachusetts Eye and Ear Infirmary
243 Charles St
Boston, MA 02114
Konstantina_stankovic@meei.harvard.edu
Phone: 617.573.3972

Abstract

Dysfunction of the inner ear is the most common cause of sensorineural hearing loss, which is the most common sensory deficit worldwide. Conventional imaging modalities are unable to depict the microanatomy of the human inner ear, hence the need to explore novel imaging modalities. We provide the first characterization of the optical properties of human cochlear sections using quantitative polarized light microscopy (qPLM). Eight pediatric cadaveric cochlear sections, aged 0 (term) to 24 months, were selected from the US National Temporal Bone Registry, imaged with qPLM and measured using Image J. Retardance of the bony otic capsule and basilar membrane were substantially higher than that of the stria vascularis, spiral ganglion neurons, organ of Corti and spiral ligament across the half turns of the spiraling cochlea. qPLM provides quantitative information about the human inner ear, and awaits future exploration *in vivo*.

1. Introduction

Hearing loss affects over 36 million Americans (National Institute on Deafness and Other Communication Disorders 2010) and 600 million people worldwide (Traynor 2014). Although majority of sensorineural hearing loss originates from the inner ear, individual cells and structure within the human inner ear cannot yet be imaged using current state-of-the-art clinical tools, including computed tomography (CT) and magnetic resonance imaging (MRI) scans. Today, the only source of information about the cellular basis of human deafness is cadaveric human temporal bones that house the inner ear. To enable future cellular-level intracochlear imaging in alive humans, we have been exploring optical imaging tools (Yang et al. 2013, Kalwani et al 2013) because optics provides high spatial resolution at a lower cost than techniques based on ionizing radiation or magnetic resonance.

We have recently demonstrated that quantitative polarized light microscopy (qPLM) detects differences in optical properties of key intracochlear structures, as evaluated using unstained mouse cochlear sections (Kalwani et al. 2013), while being faster and cheaper than immunohistochemistry. The current study explores the utility of qPLM in imaging human cochlear sections. Polarized light microscopy (PLM) is based on the principle that biological specimens alter the polarization state of the polarized light that passes through them. When the refractive index of the specimen is dependent on the polarization and direction of incoming light (a property known as birefringence), nonhomogeneous alterations in wave propagation velocity can be detected, which is referred to as sample retardance. Specimens that exhibit birefringence have directional structure, such as seen in collagen and myelin. Within hearing research, PLM has been used to examine the microcirculation within the guinea pig cochlea (Ren et al. 1993), and to study the organization of collagen within the guinea pig (Wenzel et al. 2004) and mouse (Wenzel et al. 2007) basilar membrane after laser irradiation.

Although PLM has proven useful for qualitative comparisons, qPLM has the major advantage of being quantitative. There are two key parameters in qPLM: retardance (expressed in nanometers) and the average orientation of the polarization axis with the greater index of refraction (Oldenbourg and Mei 1995). qPLM has been applied in many clinical specialties, including reproductive biology to quantify spindle aberrations in oocytes (Molinari et al. 2012), dermatology to improve detection of melanoma (Herman 2012), and orthopedics to quantify microstructural remodeling of articular cartilage following defect repair with osteochondral autograft (Raub et al. 2013). We were the first to apply qPLM to the inner ear (Kalwani et al. 2013). Specifically, we used qPLM to quantify the optical properties of sectioned cochlear tissues in two different, commonly used mouse models, C57BL/6J and CBA/CaJ. We showed that the networks of collagen fibers known to exist in mammalian cochlea are better-identified using qPLM than using conventional differential interference contrast microscopy.

Encouraged by these results in mice, which are commonly used animal models to investigate hearing and deafness, we undertook the current study to characterize the optical properties of the cadaveric human cochlear sections using qPLM, with an eye to ultimate clinical applications *in vivo*. We focused on pediatric specimens with no known pathology of the inner ear so to establish a reference for future explorations of pathologic specimens. Many diseases that cause hearing loss are characterized by defects in the quantity, quality and organization of collagen – a major birefringent molecule in the inner ear (Merchant et al. 2004, Merchant and Nadol 2010). We show that cochlear structures with the greatest retardance are the bony otic capsule and basilar membrane, suggesting that qPLM may be most useful for detecting pathology in these structures.

2. Methodology

2.1 Human cochlear sections

All neonatal human cochleas (n=79), aged between 0 (term) and 24 months, were reviewed from the Massachusetts Eye and Ear collection of the US National Temporal Bone Registry. Twenty one temporal bones reported to have normal labyrinths were selected; the remaining bones were excluded because they had signs of autolysis or otitis media. Of the 21 temporal bones with no documented cochlear histopathology, only 8 had midmodiolar sections with excellent preservation of all cells. These 8 temporal bones were therefore selected for imaging with qPLM. The average time between death and tissue fixation was 8 hours, ranging from 2 hours to 17 hours; 2 cases out of the 8 selected did not have a reported port-mortem time.

2.2 Quantitative polarized microscopy

Archival cochlear specimens that we studied had been embedded in celloidin, sectioned at 20 µm, and stained with hematoxylin and eosin as per a routine protocol (Merchant and Nadol 2010) in the US temporal bone registry. The sections were mounted onto an inverted microscope (Nikon Eclipse TE 2000-S) and imaged using a commercial birefringence microscopy system (ABRIO^{TM}; Hinds Instruments) to characterize optical anisotropy. This instrument acquires pixwelwise-resolved measurements of retardance and the orientation of the slow optical axis in the specimens, as previously described (Kalwani et al. 2013). In short, monochromatic (wavelength 546 nm) circularly polarized light travels through the specimen and a computer-controlled compensator optic. The change in state of polarization of the light wave was recorded at five different compensator settings, and sample birefringence was calculated based on a polarmetric algorithm. This system resolves retardance values to within 0.02 nm, and it accounts for light absorbance in the sample and a background correction to correct for intrinsic birefringence in the microscope optical elements. The birefringence of the following inner ear structures were measured in each of the 4 cochlear half turns: organ of Corti, stria vascularis, spiral ligament, basilar membrane, otic capsule and cell bodies of spiral ganglion neurons. The images were analyzed in ImageJ (NIH). Retardance of each cochlear structure was measured 3 times for each sample to arrive at the mean and standard error of the mean for each structure across different samples. For each cochlear structure with measured retardance, a single factor analysis of variance (ANOVA) was used (in Excel) to test the null hypothesis that the means of retardance for different cochlear turns were all equal; $p < 0.05$ was considered significant.

3. Results

Quantitative PLM of the human cochlear sections revealed differences in birefringence across cochlear structures (Figure 1, 3), and typically more structural detail than seen under simple light microscopy (Figure 2). Of the six structures measured, the otic capsule and basilar membrane were the most birefringent (Figure 4). For all structures, retardance is expressed as mean +/- standard error of the mean. Cochlear turns are analyzed from base to apex because there are well known mechanical, chemical and structural gradients along the length of the spiraling cochlea. Although there was a trend for a decreasing retardance of the otic capsule from the cochlear base toward the apex (Figure 4) – being 3.89 +/- 0.54 nm in the lower basal turn, 3.75 +/- 0.74 nm in the upper basal turn, 2.78 +/- 0.32 nm in the lower middle turn and 3.02 +/- 0.50 nm in the upper middle turn – this trend was not statistically significant (p=0.41). The basilar membrane also showed a trend toward decreasing retardance away from the cochlear base (Figure 4), being 2.25 +/-0.22 nm in the lower basal turn, 2.09 +/- 0.32 nm in the upper basal turn, 1.85 +/- 0.19 nm in the lower middle turn and 1.36 +/- 0.20 nm in the upper middle turn. However, this trend did not meet our criterion for significance (p=0.07).

The spiral ligament was the least birefringent structure in the human cochlea (Figure 4). Differences in retardance across the cochlear half turns were not statistically significant (p=0.65), being 0.52 +/-0.08 nm in the lower basal turn, 0.56 +/- 0.08 nm in the upper basal turn, 0.46 +/- 0.05 nm in the lower middle turn and 0.47 +/- 0.05 nm in the upper middle turn. Likewise, the retardance of the organ of Corti, which contains sensory hair cells, did not statistically differ across turns (p=0.99), being 0.78 +/- 0.12 nm in the lower basal turn, 0.76 +/- 0.11 nm in the upper basal, 0.80 +/- 0.16 nm in the lower middle turn and 0.78 +/- 0.13 nm in the upper middle turn. The stria vascularis, a vascular structure that generates the endocochlear potential that drives transduction current through sensory cells, was found to have a greater retardance than the organ of Corti at each half turn. Retardance of the stria vascularis did not statistically differ between turns (p=0.64), being 1.35 +/-0.16 nm in the lower basal turn, 1.20 +/- 0.14 nm in the upper basal turn, 1.11 +/- 0.11 nm in the lower middle turn, 1.12 +/- 0.15 nm in the upper middle turn. Retardance of the spiral ganglion was similar to that of the stria vascularis, and not statistically different across turns (p=0.49), being 0.97 +/-0.15 nm in the lower basal turn, 1.20 +/- 0.14 nm in the upper basal turn, 1.34 +/- 0.21 nm in the lower middle turn, 1.20 +/- 0.18 nm in the upper middle turn.

4. Discussion

To the best of our knowledge, this is the first study to characterize the optical properties of human cochlear structures using qPLM. Our results reveal that the otic capsule and basilar membrane are the most birefringent structures whereas the spiral ligament is the least birefringent cochlear structure. While the basilar membrane and the otic capsule tended to have decreasing retardance with distance away from the cochlear base – unlike the more uniform retardance of the organ of Corti, stria vascularis, spiral ligament and spiral ganglion neurons along the cochlear length– this trend did not meet our criterion for significance. The results of this study are comparable with our findings in mice (Kalwani et al. 2013). The level of retardance measured in the human otic capsule was similar to, albeit larger than that of the mouse otic capsule of different strains. However, retardance of spiral ganglion cell bodies was notably higher in humans than mice. The greatest difference between human and mouse cochlear section was in retardance of the spiral ligament, which was substantially smaller in humans than in mice. There are several possible reasons for this difference. First, mice are higher-frequency hearing animals – they can hear up to 70 kHz and have maximal sensitivity at 16 kHz whereas humans hear up to 20 Hz with the maximal sensitivity at 2 kHz. Studies in bats, which can hear up to 200 kHz, have suggested that the intricately organized collagen fibers within the spiral ligament that attach to the basilar membrane contribute to the tension in the mechanically-tuned basilar membrane, hence enabling high frequency hearing (Henson et al. 1984). Second, the time between death and cochlear extraction is substantially longer for human specimens, averaging 8 hours in our series, compared to just minutes in mice. The prolonged post-mortem time in human specimens may contribute to collagen breakdown and tissue disorganization. In addition, due to the archival nature of human specimens, they were imaged years and decades after cochlear fixation whereas mouse specimens were imaged within days of cochlear extraction; continued tissue breakdown is possible even for fixed specimens. Although our specimens were from young pediatric patients, it is relevant that the human spiral ligament begins to lose collagen-producing fibrocytes early, within the first decade of life (Wright and Schuknecht 1972), and that degeneration of the spiral ligament occurs at a faster rate than that of other cochlear structures (Kusunoki et al. 2004). In addition, fibrocytes of the spiral ligament are particularly sensitive to noise trauma and mild exposure to noise, such as seen in neonatal intensive care units, can cause hearing damage undetectable by threshold based audiogram (Wang et al. 2002).

Establishing the optical properties of normal healthy cochlear tissue is the first step in considering qPLM as a diagnostic tool *in vivo*. Although the histological sections used in this study were fixed, they are likely representative of unfixed tissue, based on our comparison of optical properties of fixed and unfixed cochlear tissues using two photon microscopy (Yang et al. 2013). By establishing a normal baseline, out study enables future interpretation of pathologic human specimens, and classification of pathologies that are reflected in abnormal qPLM signatures. Many human diseases are characterized by disorganization or malfunction of collagen in the inner ear (Merchant and Nadol 2010), including Alport's disease (Merchant et al. 2004), otosclerosis, osteogenesis imperfect and Paget's disease.

Our study indicates that qPLM is capable of providing quantitative details of human cochlear structures, in particular the organization of collagen networks. Future studies are needed to explore whether application of qPLM *in vivo* could detect fine pathologic changes early, thus enabling early treatment and possible prevention of hearing loss. Combining qPLM with optical coherence tomography (OCT) may be particularly promising because OCT can generate cross-sectional images with a high spatial resolution based on back-scattered light from a focused beam of infrared light directed at the tissue (Huang et al. 1991). The resolution of OCT can range from 2-15 μm (Drexler et al. 2001), which has been sufficient to visualize the microanatomy of the rat cochlea *ex vivo* (Wong et al. 2000; Wong et al. 2004) and the mouse cochlea *in vivo* (Subhash et al, 2010), revealing the three cochlear fluid-filled spaces, modiolus, spiral ligament, the organ of Corti and spiral limbus.

Polarization-sensitive OCT (PS-OCT) combines qPLM and OCT, thus allowing measurement of the birefringence and the orientation of the fast axis of a specimen. This generates a quantitative 3D cross sectional image of a specific region of interest. PS-OCT has allowed identification of pathological microstructural changes in the concentration and organization of various tissue types such as tendons and ligaments in the knee (Martin et al. 2003; Bagnaninchi et al. 2010), and vocal folds of the larynx (Burns et al. 2009). PS-OCT has been used during laryngeal surgery to provide immediate feedback (Burns et al. 2009), and identify scar tissue within vocal folds to enable precise treatment of the scar tissue that contributes to dysphonia (Kim et al. 2010). It would be important to explore whether PS-OCT could similarly generate 3D cross sectional images of the inner ear *in vivo*, hence providing diagnostic information and invaluable real-time feedback during inner-ear surgery. Such feedback is currently not available but may be crucial in preventing microstructural damage and the associated hearing loss during procedures such as cochlear implantation, stapedectomy or labyrinthectomy. PS-OCT may also enable precise delivery of emerging cell-based and genetic therapies to the diseased regions of the inner ear, and quantitative monitoring of the response to treatment.

A limitation of our study is that it is based on healthy neonatal cochlear sections so that further research is required to explore birefringent patterns in other age groups and in pathological states. Nonetheless, our study highlights the utility of qPLM in visualizing human cochlear structures, and suggests that PS-OCT may be a useful tool to investigate the inner ear and guide precise therapy.

5. Conclusions

This study provides the first characterization of the optical properties of the microstructures within the human cochlea using qPLM. We note many similarities between the retardance of the human and mouse cochlear tissues, with the notable exception of the spiral ligament, which is much less birefringent in humans than in mice. Taken together, this suggests that techniques developed in mice will have quantitative utility in humans. Our measurements of normal human tissue motivate future exploration of qPLM in diseased tissue associated with hearing loss so to determine whether birefringence can serve as an imaging biomarker for inner ear diseases that are currently lumped under the umbrella term “sensorineural hearing loss”. Our results, combined with others’ reports of intracochlear imaging using OCT in rodent models, suggest that PS-OCT may have multiple applications in micro-structural diagnosis and targeted therapy of disorders of the human inner ear, while providing real-time feedback during surgical intervention.

Acknowledgments

We are grateful for support by NIDCD grant K08DC010419 (K.M.S.), the Bertarelli Foundation (K.M.S.), and Curing Kids Foundation at Massachusetts Eye and Ear (K.M.S.).

Bibliography

Bagnaninchi PO, Yang Y, Bonesi M, et al. (2010) In-depth imaging and quantification of degenerative changes associated with Achilles ruptured tendons by polarization-sensitive optical coherence tomography. Phys Med Biol 55:3777–3787. doi: 10.1088/0031-9155/55/13/014

Burns JA, Kim KH, Kobler JB, et al. (2009) Real-time tracking of vocal fold injections with optical coherence tomography. Laryngoscope 119:2182–2186. doi: 10.1002/lary.20654

Burns JA, Zeitels SM, Anderson RR, et al. (2005) Imaging the mucosa of the human vocal fold with optical coherence tomography. Ann Otol Rhinol Laryngol 114:671–676.

Drexler W, Morgner U, Ghanta RK, et al. (2001) Ultrahigh-resolution ophthalmic optical coherence tomography. Nat Med 7:502–507. doi: 10.1038/86589

Herman C (2012) Emerging technologies for the detection of melanoma: achieving better outcomes. Clin Cosmet Investig Dermatol 5:195–212. doi: 10.2147/CCID.S27902

Huang D, Swanson EA, Lin CP, et al. (1991) Optical coherence tomography. Science 254:1178–1181.

Kalwani NM, Ong CA, Lysaght AC, et al. (2013) Quantitative polarized light microscopy of unstained mammalian cochlear sections. J Biomed Opt 18:26021. doi: 10.1117/1.JBO.18.2.026021

Kashtan CE (1999) Alport syndrome. An inherited disorder of renal, ocular, and cochlear basement membranes. Medicine (Baltimore) 78:338–360.

Kim KH, Burns JA, Bernstein JJ, et al. (2010) In vivo 3D human vocal fold imaging with polarization sensitive optical coherence tomography and a MEMS scanning catheter. Opt Express 18:14644–14653.

Kusunoki T, Cureoglu S, Schachern PA, et al. (2004) Age-related histopathologic changes in the human cochlea: a temporal bone study. Otolaryngol Head Neck Surg 131:897–903. doi: 10.1016/j.otohns.2004.05.022

Liapis H, Jain S (2013) The interface of genetics with pathology in alport nephritis. J Am Soc Nephrol 24:1925–1927. doi: 10.1681/ASN.2013080913

Martin SD, Patel NA, Adams SB Jr, et al. (2003) New technology for assessing microstructural components of tendons and ligaments. Int Orthop 27:184–189. doi: 10.1007/s00264-003-0430-4

Merchant SN, Burgess BJ, Adams JC, et al. (2004) Temporal bone histopathology in alport syndrome. Laryngoscope 114:1609–1618. doi: 10.1097/00005537-200409000-00020

Molinari E, Evangelista F, Racca C, et al. (2012) Polarized light microscopy-detectable structures of human oocytes and embryos are related to the likelihood of conception in IVF. J Assist Reprod Genet 29:1117–1122. doi: 10.1007/s10815-012-9840-9

Nakashima T, Naganawa S, Sone M, et al. (2003) Disorders of cochlear blood flow. Brain Res Brain Res Rev 43:17–28.

National Institute on Deafness and Other Communication Disorders (2010) Quick Statistics.

Raub CB, Hsu SC, Chan EF, et al. (2013) Microstructural remodeling of articular cartilage following defect repair by osteochondral autograft transfer. Osteoarthr Cartil 21:860–868. doi: 10.1016/j.joca.2013.03.014

Ren T, Lin X, Nuttall AL (1993) Polarized-light intravital microscopy for study of cochlear microcirculation. Microvasc Res 46:383–393. doi: 10.1006/mvre.1993.1061

Rubel D, Kruegel J, Martin M, et al. (2014) Collagen receptors integrin alpha2beta1 and discoidin domain receptor 1 regulate maturation of the glomerular basement membrane and loss of integrin alpha2beta1 delays kidney fibrosis in COL4A3 knockout mice. Matrix Biol. doi: 10.1016/j.matbio.2014.01.006

Storey H, Savige J, Sivakumar V, et al. (2013) COL4A3/COL4A4 mutations and features in individuals with autosomal recessive Alport syndrome. J Am Soc Nephrol 24:1945–1954. doi: 10.1681/ASN.2012100985

Thorner PS (2007) Alport syndrome and thin basement membrane nephropathy. Nephron Clin Pract 106:c82–88. doi: 10.1159/000101802

Wang Y, Hirose K, Liberman MC (2002) Dynamics of noise-induced cellular injury and repair in the mouse cochlea. J Assoc Res Otolaryngol 3:248–268. doi: 10.1007/s101620020028

Wenzel GI, Anvari B, Mazhar A, et al. (2007) Laser-induced collagen remodeling and deposition within the basilar membrane of the mouse cochlea. J Biomed Opt 12:021007. doi: 10.1117/1.2714286

Wenzel GI, Pikkula B, Choi C-H, et al. (2004) Laser irradiation of the guinea pig basilar membrane. Lasers Surg Med 35:174–180. doi: 10.1002/lsm.20091

Wolman M (1975) Polarized light microscopy as a tool of diagnostic pathology. J Histochem Cytochem 23:21–50.

Wong BJ, de Boer JF, Park BH, et al. (2000) Optical coherence tomography of the rat cochlea. J Biomed Opt 5:367–370. doi: 10.1117/1.1310165

Wong BJ f, Zhao Y, Yamaguchi M, et al. (2004) Imaging the internal structure of the rat cochlea using optical coherence tomography at 0.827 microm and 1.3 microm. Otolaryngol Head Neck Surg 130:334–338. doi: 10.1016/j.otohns.2003.11.007

Wong BJF, Jackson RP, Guo S, et al. (2005) In vivo optical coherence tomography of the human larynx: normative and benign pathology in 82 patients. Laryngoscope 115:1904–1911. doi: 10.1097/01.MLG.0000181465.17744.BE

Wright JL, Schuknecht HF (1972) Atrophy of the spiral ligament. Arch Otolaryngol 96:16–21.

Yang X, Pu Y, Hsieh C-L, et al. (2013) Two-photon microscopy of the mouse cochlea in situ for cellular diagnosis. J Biomed Opt 18:031104.

Zehnder AF, Adams JC, Santi PA, et al. (2005) Distribution of type IV collagen in the cochlea in Alport syndrome. Arch Otolaryngol Head Neck Surg 131:1007–1013. doi: 10.1001/archotol.131.11.1007

Oldenbourg R, Mei G. New polarized light microscope with precision universal compensator. J. Microsc. 180(2), 140–147 (1995).

Schuknecht's Pathology of the Ear, 3rd edn. S Merchant, J Nadol. McGraw-Hill Education (UK), 2010.

Henson MM, Henson OW Jr, Jenkins DB. The attachment of the spiral ligament to the cochlear wall: anchoring cells and the creation of tension. Hear Res. 1984;16(3):231-42.

H. M. Subhash, V. Davila, H. Sun et al, "Volumetric in vivo imaging of intracochlear microstructures in mice by highspeed spectral domain optical coherence tomography," J. Biomed. Opt. 15: 036024 (2010).

B. Traynor, "The incidence of hearing loss around the world." Hearing International. http://hearinghealthmatters.org/hearinginternational/2011/incidence-of-hearing-loss-around-the-world/ (July 2014)

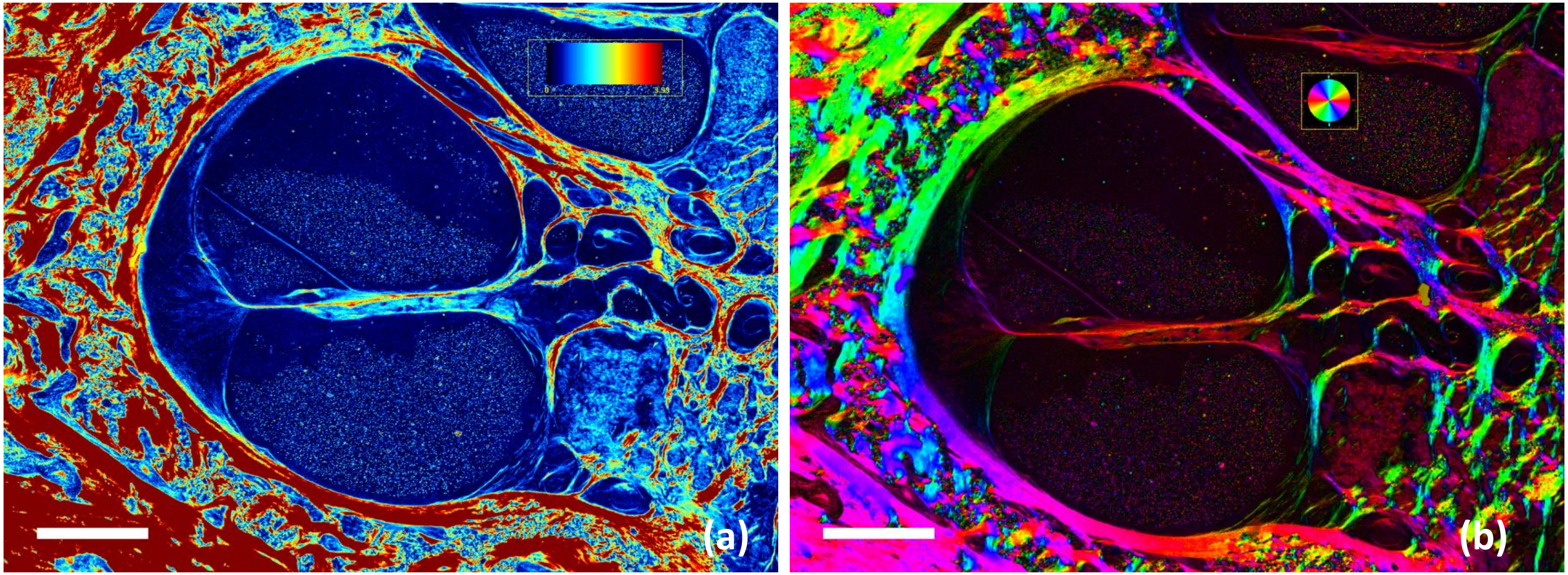

Fig. 1 (a) Pseudocolour retardance magnitude and (b) orientation image of a cross-section through the upper basal turn of a human cochlea. The colored bar in (a) indicates the scale for retardance magnitude from 0 to 3.99 nm. The colored circle in (b) indicates the correspondence between pixel colour and orientation of the slow axis. White scale bar: 500μm.

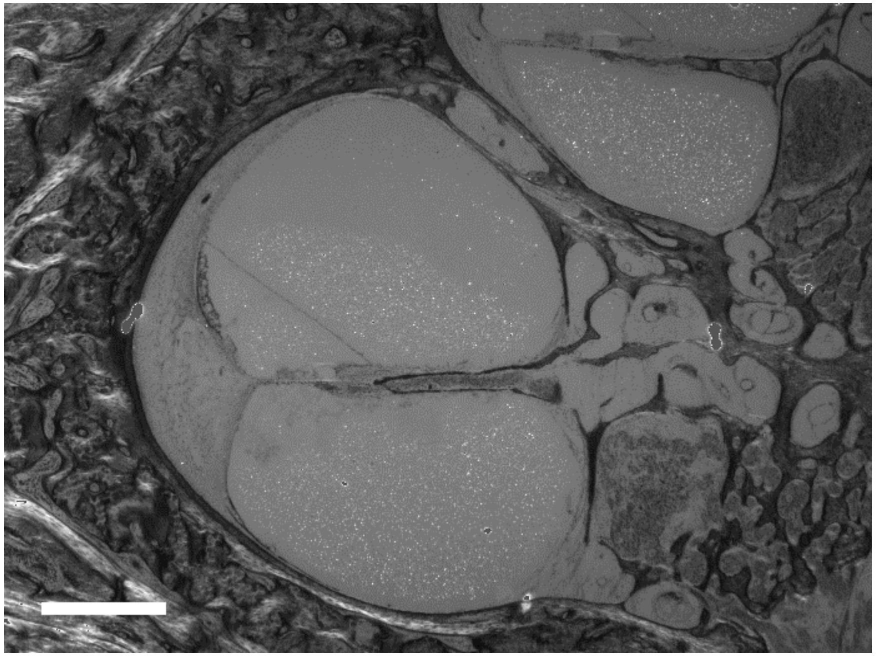

Fig. 2 Image of a cross-section through the upper basal turn of a human cochleam (same as in Fig. 1) under simple light microscopy. White scale bar: 500 µm.

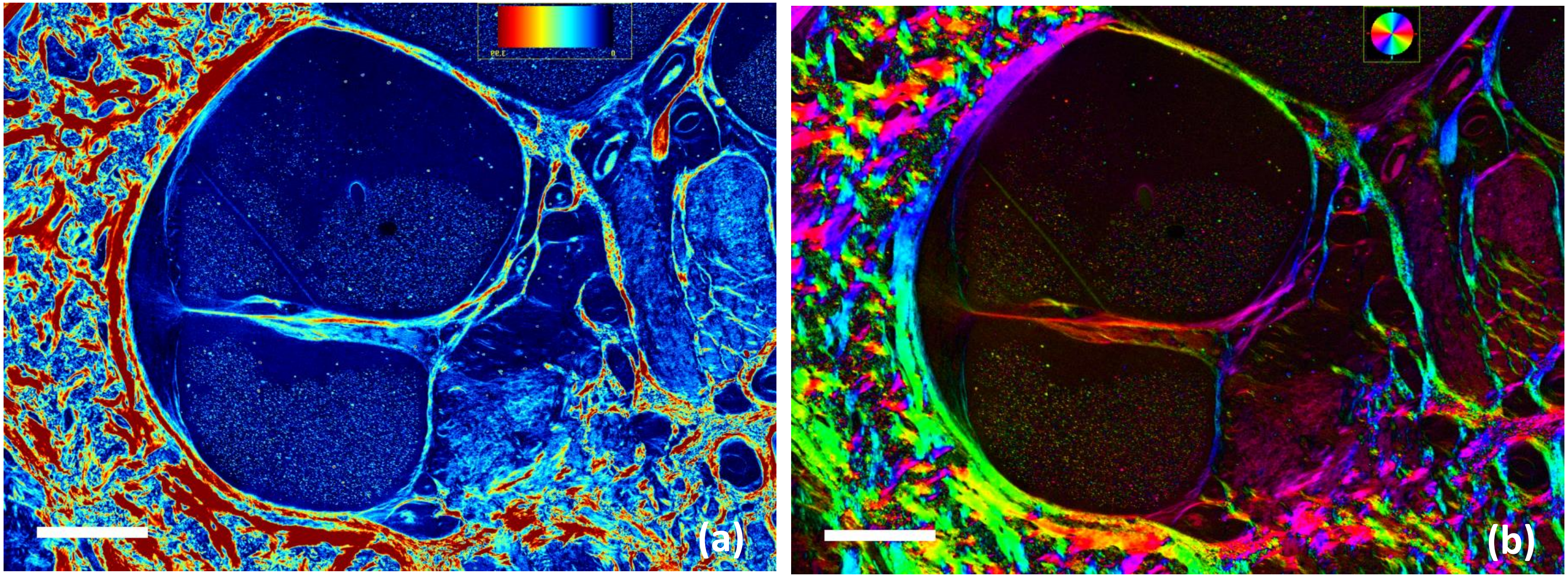

Fig. 3 (a) Pseudocolour retardance magnitude and (b) orientation image of a cross-section through the lower basal turn of a human cochlea. The colored bar in (a) indicates the scale for retardance magnitude from 0 to 3.99 nm. The colored circle in (b) indicates the correspondence between pixel colour and orientation of the slow axis. White scale bar: 500 µm.

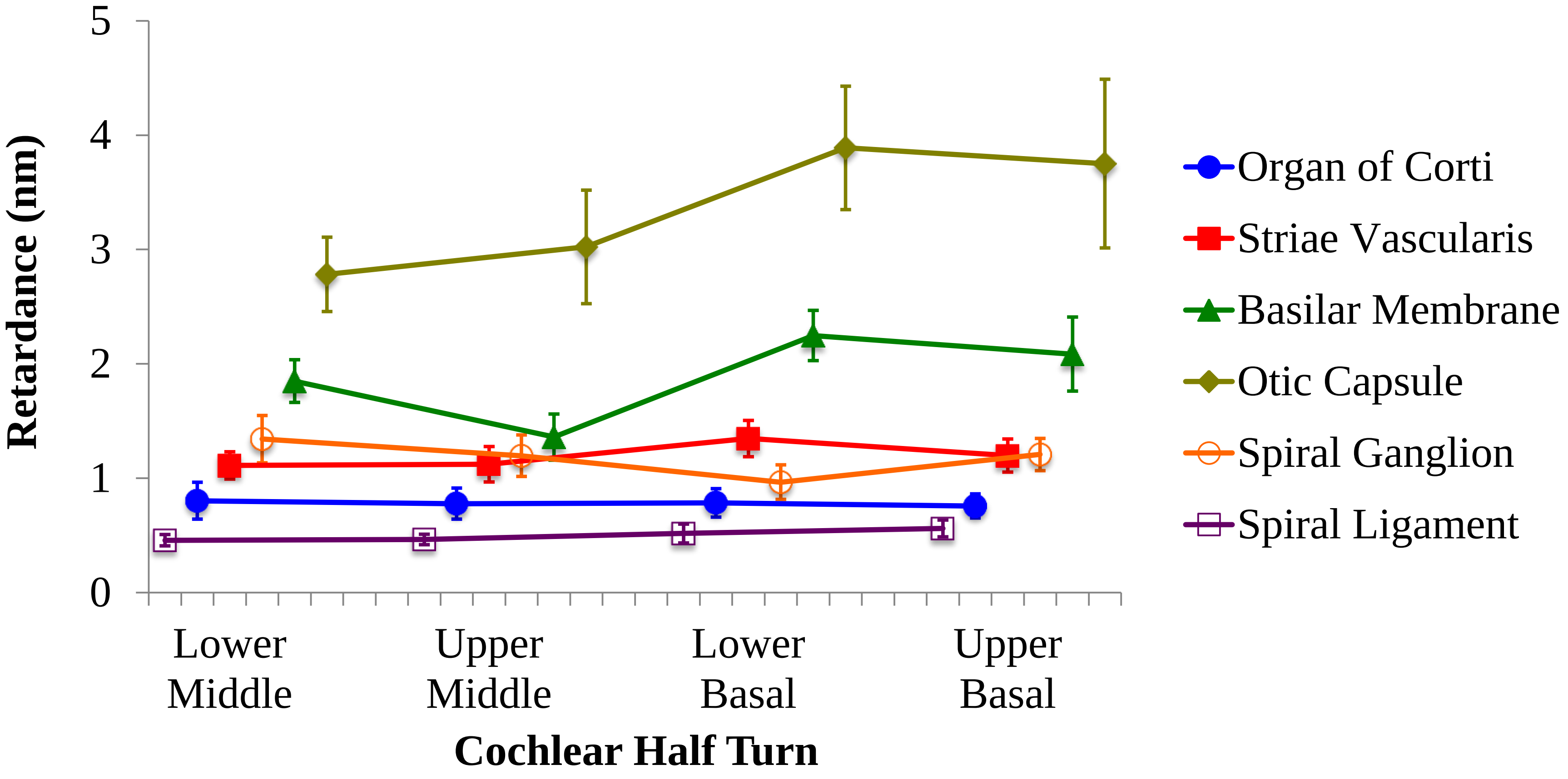

Fig. 4 Retardance of cochlear structures along the cochlear length, from the lower basal to the upper middle turn. The horizontal axis is slightly shifted for each cochlear tissue to facilitate comparison.